Chinese Physics Letters

LETTER

Medium Electrical Conductivity Governs the Collective Behaviors of Quincke Rollers

Cite as: Zihan Qiao *et al*. 2026 *Chin. Phys. Lett.* **43** 100901

Recommended Articles

The Surprising Physics of Interfaces in Active Matter
Alexandre Solon, and Yongfeng Zhao
Chin. Phys. Lett. **42**, 100901 (2025)

Experimental Verification of Intrinsic Pressure Framework in an Activity Landscape
Zihao Sun, Longfei Li, Chuyun Wang, Jing Wang, Huaicheng Chen, Gao Wang, Fangfu Ye, Liyu Liu, and Mingcheng Yang
Chin. Phys. Lett. **43**, 010901 (2026)

A Quorum Sensing Active Matter in a Confined Geometry
Yuxin Zhou, Yunyun Li, and Fabio Marchesoni
Chin. Phys. Lett. **40**, (2023)

Tunable Memory and Activity of Quincke Particles in Micellar Fluid
Yang Yang, Meng Fei Zhang, Lailai Zhu, and Tian Hui Zhang
Chin. Phys. Lett. **40**, (2023)

A series journal of Chinese Physical Society distributed by IOP Publishing

Chinese Physics Letters

Chin. Phys. Lett. **43** 100901 (2026)

LETTER

DOI: 10.1088/0256-307X/43/10/100901
CSTR: 32039.14.0256-307X.43.10.100901

Medium Electrical Conductivity Governs the Collective Behaviors of Quincke Rollers

Zihan Qiao(乔子涵)[1], Jingrui Gu(顾京瑞)[1], Jiayu Liu(刘佳钰)[1], Guomeng Wang(王国猛)[1], Hao Lu(卢灏)[2], Ting Kuang(况婷)[3], Bo Zhang(张波)[2,*], and Wei Wang(王威)[1,*]

[1]School of Materials Science and Engineering, Harbin Institute of Technology (Shenzhen), Shenzhen 518055, China
[2]Department of Physics, National Laboratory of Solid State Microstructure and Collaborative Innovation Center of Advanced Microstructures, Nanjing University, Nanjing 210093, China
[3]Education Center of Experiments and Innovations (Analysis and Testing Center), Harbin Institute of Technology (Shenzhen), Shenzhen 518055, China

[*]Corresponding authors. Email: bz@nju.edu.cn; weiwangsz@hit.edu.cn

Active matter systems can convert environmental energy into continuous motion and exhibit collective behaviors. As a typical electrically driven active particle system, Quincke rollers can display a variety of collective behaviors under a uniform DC electric field. However, a systematic understanding of the emergence and evolution of different collective behaviors is still lacking, and it remains unclear how external environmental conditions, such as temperature and humidity, influence the dynamics of collective behaviors. In this work, we find that increasing temperature and humidity drives a continuous transition of the collective behavior of Quincke rollers from vortices to polar clusters, rotating clusters, and finally active crystals. *In situ* electrical measurements show that the medium conductivity increases by nearly 10-fold as the temperature rises from 20 ℃ to 60 ℃, and by approximately 30-fold as the relative humidity increases from 5% to 65%, whereas the permittivity changes by about 10−15%. Finite-element calculations further reveal that the increase in medium electrical conductivity strongly modifies the magnitudes of the electric dipolar and hydrodynamic interactions between rollers. These forces shift from pure repulsion to anisotropic attraction and then to isotropic attraction, resulting in the emergence of vortices, polar clusters, rotating clusters, and active crystals in turn. These results provide a simple physical picture linking the conductivity of the medium to the collective states in Quincke roller system and establish a theoretical framework that incorporates dipolar interaction, hydrodynamic interaction, and electro-hydrodynamic interaction for understanding the dynamics of collective behavior. In addition, this work demonstrates that temperature and humidity can serve as simple, efficient, and reversible control parameters for the *in situ* regulation of the collective behaviors of Quincke rollers.

Introduction

Active matter systems are intrinsically out-of-equilibrium systems that continuously convert environmental energy into autonomous motion. Because of the complex self-organized behaviors that emerge at the collective scale, active matter has become a central topic at the interface of soft matter physics and biophysics [1−3]. From the coordinated flight of bird flocks to the collective migration of bacterial colonies, natural active systems exhibit highly adaptive collective behaviors. In artificial systems, model platforms such as self-propelled colloids, light-driven micromotors, and electrically driven particles provide controllable systems for the quantitative study of these phenomena [4−6].

Among them, Quincke rollers driven by a uniform DC electric field have attracted particular attention because they can spontaneously break symmetry without directional guidance from the external field and generate a variety of collective behaviors [7−10]. The mechanism of Quincke rollers originates from the classical Quincke rotation effect [11]. When an insulating sphere separated in a weakly conductive liquid is subjected to an external electric field E_0, any small perturbation can destabilize the electric dipole of the particle once the field strength exceeds the critical value E_Q. This spontaneous symmetry breaking generates the electric torque, causing the sphere to rotate steadily around an axis perpendicular to E_0. In the presence of a solid boundary, this rotation is converted into horizontal motion [12]. Quincke rollers have been reported to exhibit a variety of collective behaviors, including directional motion [13,14], vortices [15−17], rotating clusters [16,18], and active crystals [12,19].

However, a complete understanding of why these collective states emerge or how transitions occur between different states is still lacking. In fact, different research groups, and even the same group at different times, could observe very different collective behaviors under seemingly identical experimental conditions. This suggests that, in addition to conventional control parameters such as the applied electric field strength and 2D area fraction, there are other hidden variables that are overlooked but have a critical influence on interparticle interactions.

For example, temperature (T) and relative humidity (RH) could be such hidden yet critical variables. In particular, the electrical properties of weakly conductive liquid media commonly used in Quincke systems, such as hexadecane containing surfactant, are highly sensitive to environmental temperature and humidity [20]. Earlier studies have also occasionally reported the influence of humidity on Quincke rollers, such as the "hovering" state [7] observed under extremely dry conditions and the formation of large stable aggregates [21] at high humidity. However, these studies mainly remained at the phenomenological level. They neither systematically explored the full phase space generated by continuous changes in temperature and humidity, nor established a quantitative relationship between collective behaviors and environmental conditions. One possible reason for this gap in theoretical understanding is that the variation of the underlying interparticle interactions remains poorly understood.

In this Letter, we systematically vary the environmental temperature and humidity and find that, as the RH increases from 5% to 65% or the temperature rises from 20 ℃ to 60 ℃, the system successively transitions among four typical collective states: vortex, polar cluster, rotating cluster, and active crystal. Through *in situ* measurements, we find that the medium conductivity is strongly enhanced by increasing

Received 12 June 2026; accepted 13 September 2026; published 5 November 2026
© 2026 Chinese Physical Society and IOP Publishing Ltd. All rights, including for text and data mining, AI training, and similar technologies, are reserved.

Check for updates

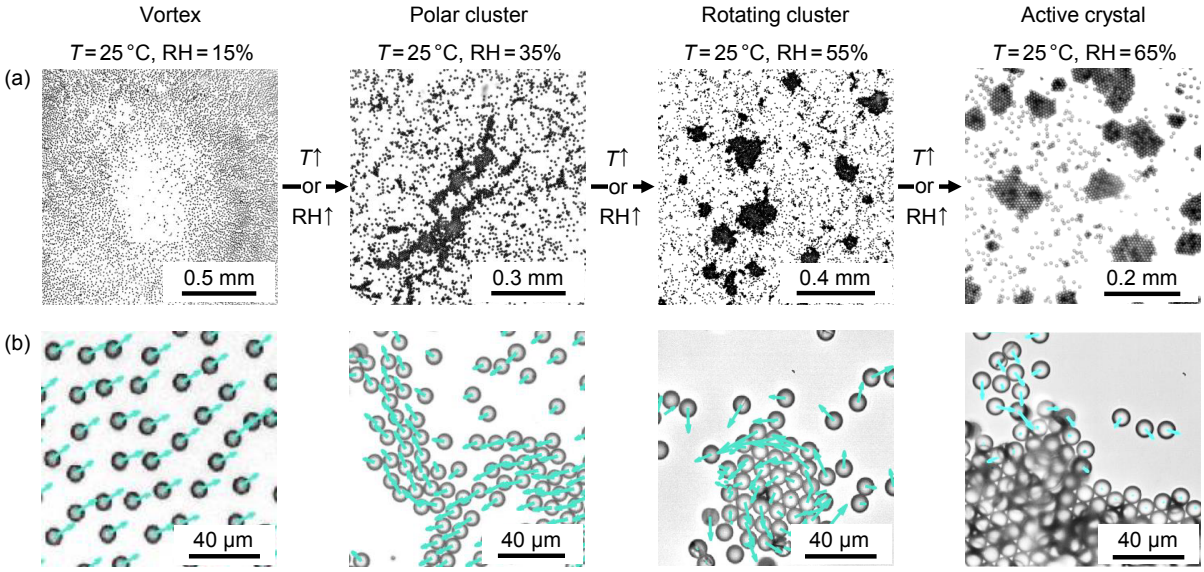

Fig. 1. Collective behaviors of Quincke rollers upon increasing T and/or RH. Optical micrographs of each state: (a) at low magnification and (b) at high magnification. Arrows in (b) represent individual particle velocities.

either temperature or humidity, whereas the permittivity increases only weakly. This result indicates that medium electrical conductivity is the dominant factor controlling the evolution of collective behaviors under different temperatures or humidities. Furthermore, quantitative modeling demonstrates that as the medium electrical conductivity increases, the inter-roller interaction transitions from being dominated by isotropic dipolar repulsion to being dominated by anisotropic attraction and eventually evolves into isotropic hydrodynamic attraction. Concurrently, the position of the interaction potential energy minimum decreases, which is in qualitative agreement with the experimental observations that rollers are packed more closely at high temperature or humidity. These results reveal that temperature and humidity impact the collective behaviors by modifying the pairwise interactions of Quincke rollers through changes in medium conductivity. Beyond the specific cases of temperature and humidity, this work establishes a theoretical framework based on pairwise interaction forces for understanding the collective behaviors of Quincke rollers.

Transitions of Collective Behaviors by Changing Temperature and Humidity

At a fixed electric field strength E, different collective behaviors of Quincke rollers were observed under different temperatures T and RHs [Figs. 1(a)–1(c)], including vortex, polar cluster, rotating cluster, and active crystal state [see the Supplementary Materials (SM), Movie 1]. Below, we use the case of increasing RH as an example while keeping T at 25 ℃. The case of increasing T shows qualitatively the same transition and is not shown here.

The vortex state typically appears at low humidity (e.g., RH = 15%) or low temperature (e.g., T = 25 ℃). In this state, a large number of rollers self-organize into a single vortex or multiple vortices. The particles in a vortex are relatively dispersed; their velocities are highly aligned. As humidity increases, the vortex state first transforms into a polar cluster state (e.g., RH = 35%), where rollers form elongated clusters that move along the long axis. At an even higher humidity (e.g., RH = 55%), the system evolves into a rotating cluster state, where the rollers aggregate into a compact cluster that spins. Under high humidity conditions (e.g., RH = 65%), rollers form an active crystal state, characterized by an ordered 2D hexagonal close-packed structure. In this state, the particles in the center of the crystal are nearly immobile, while the particles at the edge of the crystal exchange with the rollers outside. To summarize, upon raising RH and/or T, a population of Quincke rollers evolves from a vortex to a polar cluster, a rotating cluster, and finally an active crystal state, with the average interparticle distance gradually decreasing. The dynamics are characterized by two distinct timescales: the system stabilizes over approximately 1–3 min upon a change in T or RH, whereas the collective state responds and evolves within a few seconds. Unless the environmental conditions change, the collective states remain stable for at least 10 min.

We further constructed the state diagrams of the collective behaviors in the humidity–E plane [Fig. 2(a)] and in the temperature–E plane [Fig. 2(b)]. The state diagrams show that, in the range of E = 2.28–3.42 V·μm^{-1}, increasing RH from 5% to 65% or increasing T from 20 ℃ to 60 ℃ drives the collective state successively from vortex to polar cluster, rotating cluster, and active crystal. Similarly, at fixed T or RH, decreasing the electric field strength induces the same sequence of phase transitions, consistent with previous reports that the electric field strength can modulate collective behavior and induce multiple phase transitions [19,22] as well as with the sequence observed under varying pulse duration and interval [16]. Notably, this transition process is reversible. When cooling the heated system to below 25 ℃ or reducing the RH of the moisture-exposed system to below 25%, the system traverses the four states in reverse, ultimately recovering the vortex state. At low E and high RH or T, the system enters the subcritical state, where rollers stop moving and aggregate into immotile clusters due to the increased activation threshold with increasing RH or T (see below).

Taking E = 2.86 V·μm^{-1} as an example, we also constructed a T–RH phase diagram [Fig. 2(c)]. It demonstrates a synergistic effect between T and RH; for instance, increasing the RH from 25% to 45% at T = 30 ℃ yields the same state as increasing the T from 30 ℃ to 50 ℃ at RH = 25%. Additionally, at the low-T and low-RH limit (20 ℃, 5% RH), we observed an oscillatory state that is not marked in the phase diagram. This phenomenon originates from the charge-injection layer becoming comparable to the particle radius under high E and low carrier density n_0 (caused by low T and RH) [23,24]. However, under most of the conditions used throughout this study, the charge-injection layer remains much thinner than the particle radius, and its effect can therefore be neglected in the following discussions.

The electric field strength threshold E_Q in the experiment is 1.28 V·μm^{-1} under the specific conditions of 25 ℃ and 15% RH. Note that the value of E_Q varies with changes in environmental T and RH. Therefore, the E_Q values under other experimental conditions can be

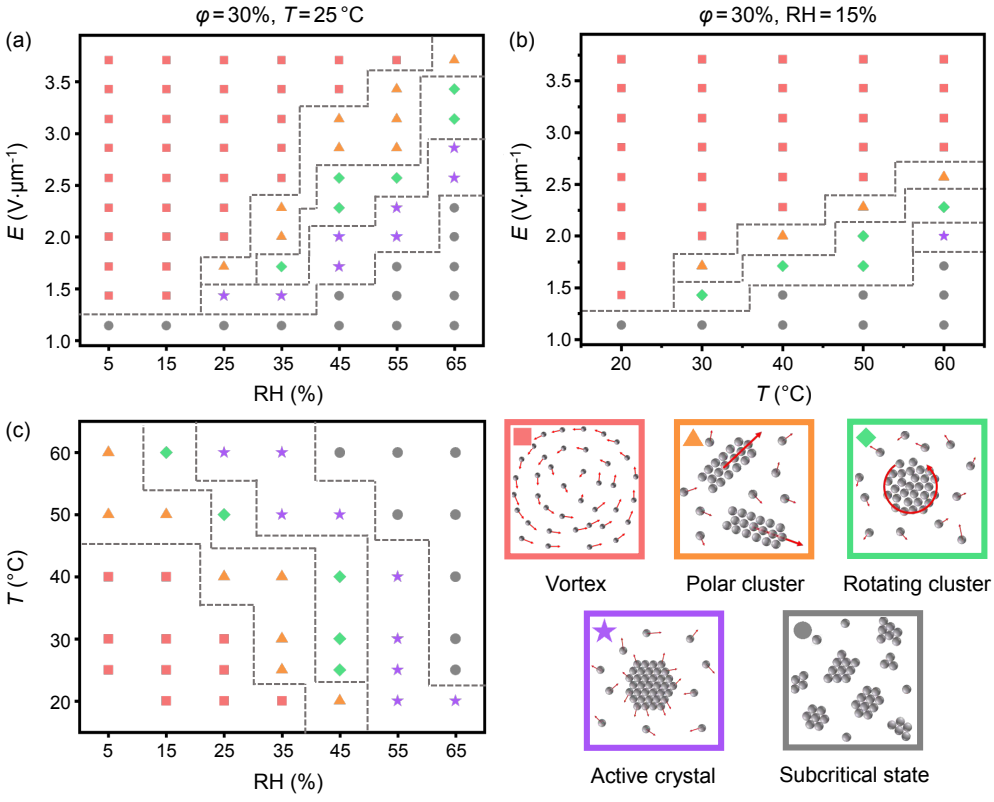

Fig. 2. State diagrams of the collective behaviors of Quincke rollers under different (a) humidities, (b) temperatures, and (c) humidity/temperature conditions. Grey circles, purple stars, green diamonds, orange triangles, and red squares represent the subcritical state, active crystal, rotating cluster, polar cluster, and vortex state, respectively.

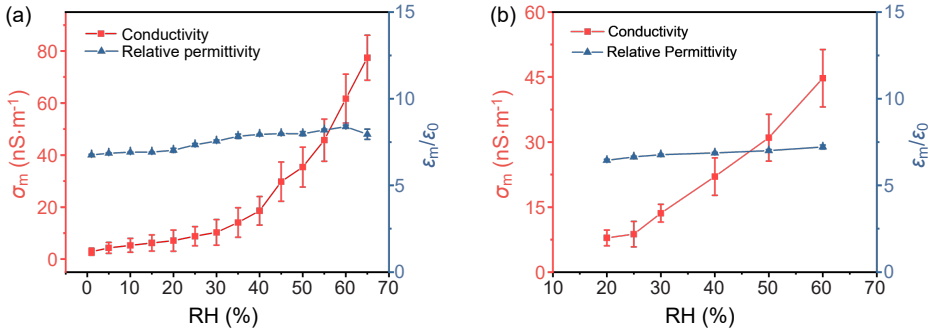

Fig. 3. Variations of the medium electrical conductivity σ_m and electrical permittivity ε_m at (a) different relative humidities, measured at $T = 25$ ℃, and (b) different temperatures, measured at RH = 15%. Error bars in (a) and (b) represent standard deviations from three replicates.

inferred from the boundary between the subcritical states and other active cluster phases under different conditions in Fig. 2.

Temperature and Humidity Modify the Electrical Properties of the Medium

It is known that the single-particle dynamics of a Quincke roller, especially the threshold electric field strength for rotation, E_Q, is affected by the electrical properties of the medium and the particle [7],

$$E_Q^2 = \frac{2\sigma_m\mu_m(R+2)^2}{3\varepsilon_m^2(S-R)},\quad R = \frac{\sigma_p}{\sigma_m},\quad S = \frac{\varepsilon_p}{\varepsilon_m}, \tag{1}$$

where σ_m and ε_m are the electrical conductivity and permittivity of the medium, respectively, σ_p and ε_p are the electrical conductivity and permittivity of the particle, and μ_m is the dynamic viscosity of the medium. In our system, the particle conductivity [$\sigma_p \sim 10^{-15}$ S·m^{-1} for polystyrene (PS)] [7] is much smaller than the medium conductivity [$\sigma_m \sim 10^{-8}$ S·m^{-1} of dioctyl sulfosuccinate sodium salt (AOT)/hexadecane] [25,26], so that $\sigma_p \ll \sigma_m$. Therefore, $R \approx 0$, and Eq. (1) can be simplified as

$$E_Q^2 \approx \frac{8\sigma_m\mu_m}{3\varepsilon_m\varepsilon_p}. \tag{2}$$

Owing to the high glass transition temperature (95 ℃) and hydrophobicity of PS, σ_p and ε_p remain essentially unchanged with T and RH in the tested range [27]. Moreover, μ_m is insensitive to humidity and depends weakly on temperature (see Sec. 5 and Fig. S5 of the SM). Therefore, we focus on the changes in σ_m and ε_m under different T and RH. The results in Fig. 3 show that increasing T and RH causes a large increase in σ_m but not in ε_m. Specifically, when RH increases from 5% to 65%, σ_m increases by nearly 30×, from 2.7 nS·m^{-1} to 79.6 nS·m^{-1} [Fig. 3(a)]. Similarly, when T increases from 20 ℃ to 60 ℃, σ_m increases by nearly 10×, from 4.7 nS·m^{-1} to 46.8 nS·m^{-1} [Fig. 3(b)]. In contrast, ε_m changes with T and RH by only 9.6% and 14.2%, respectively, under the same conditions. Similar changes in σ_m and ε_m have been reported in other systems containing reverse micelles of AOT [28,29]. The large increase in σ_m was due to

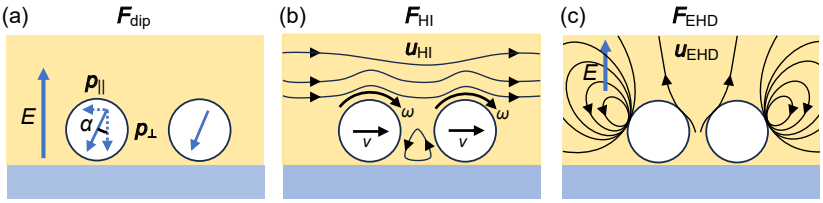

Fig. 4. Schematic of the pairwise interactions between two Quincke rollers. (a) Electrical dipolar interaction $\boldsymbol{F}_{\rm dip}$. α is the dipole tilt angle; $\boldsymbol{p}_{\parallel}$ and $\boldsymbol{p}_{\perp}$ represent dipole components parallel to $\boldsymbol{v}$ and perpendicular to $\boldsymbol{v}$ but parallel to $\boldsymbol{E}$, respectively. (b) Hydrodynamic interaction $\boldsymbol{F}_{\rm HI}$. ω and $\boldsymbol{v}$ represent the rollers' angular velocity and translational velocity, respectively. (c) EHD flow interaction $\boldsymbol{F}_{\rm EHD}$. Thin black lines show flow streamlines.

the enhanced dissociation of AOT and increased charging of the reverse micelles [30]. On the other hand, $\varepsilon_{\rm m}$ is only weakly affected because the water content remains at trace levels and the temperature variation is moderate, so that AOT reverse micelles do not form extensive, percolation-like connections. To summarize, our *in situ* electrical measurements suggest that a significant rise in $\sigma_{\rm m}$ upon raising RH or T could be a major contributor to the change in the collective behaviors of Quincke rollers.

Mechanism of How Electrical Conductivity Influences the Collective Behaviors of Quincke Rollers

To understand how changes in $\sigma_{\rm m}$ modify the interactions between rollers and thus lead to a change in their collective behaviors, we note that Quincke rollers interact through three major forces (Fig. 4): dipolar interaction (dip) [31–33], electrohydrodynamic interaction (EHD) [34–38], and hydrodynamic interaction (HI) due to rotations [18,39]. Importantly, the magnitudes and directions of all three change significantly with $\sigma_{\rm m}$. Below, we calculate the interaction forces between a pair of rollers as a function of $\sigma_{\rm m}$ and show how the results qualitatively explain the transition among the four collective behaviors upon changing humidity or temperature.

1. Dipolar Forces $\boldsymbol{F}_{\rm dip}$
   Under an external electric field $\boldsymbol{E}$, Quincke rollers acquire an effective dipole moment $\boldsymbol{p}_{\rm eff}$, which generates a dipolar interaction force $\boldsymbol{F}_{\rm dip}$ between rollers (see Sect. S3.1 of the SM for details). For stationary, poorly conductive particles, the dipoles are antiparallel to $\boldsymbol{E}$, resulting in pairwise repulsion. When the rollers roll, however, charge relaxation inside the insulating particles lags behind the external field, causing the dipole to tilt by an angle α relative to $\boldsymbol{E}$. As a result, the dipole can be decomposed into $\boldsymbol{p}_{\parallel}$ parallel to the particle velocity $\boldsymbol{v}$ [Fig. 4(a)], which produces a head-to-tail dipolar attraction between neighboring rollers [31,32], and $\boldsymbol{p}_{\perp}$ parallel to $\boldsymbol{E}$ but perpendicular to $\boldsymbol{v}$, which produces an isotropic dipolar repulsion. These interactions depend on the center-to-center distance $\boldsymbol{r}$ between neighboring rollers. In addition, partial ion dissociation from the surfactant AOT generates an electrical double layer (EDL) around the particle surface, which strongly screens the dipolar interaction. After accounting for this EDL screening, the attractive and repulsive dipolar forces between two neighboring Quincke rollers are [40]

$$\boldsymbol{F}_{\rm dip_att.} = -(\kappa h \mathrm{e}^{-\kappa h})\frac{3}{2\pi\varepsilon_{\rm m}}\frac{\boldsymbol{p}_{\parallel}^2}{r^4}\hat{\boldsymbol{r}}, \tag{3}$$

$$\boldsymbol{F}_{\rm dip_rep.} = (\kappa h \mathrm{e}^{-\kappa h})\frac{3}{4\pi\varepsilon_{\rm m}}\frac{\boldsymbol{p}_{\perp}^2}{r^4}\hat{\boldsymbol{r}}, \tag{4}$$

where $h = r - 2a$ is the surface-to-surface distance between particles, $\hat{\boldsymbol{r}} = \boldsymbol{r}/r$ is the unit vector in the direction of $\boldsymbol{r}$, $\kappa = 1/\lambda_{\rm D}$ is the Debye screening parameter, and the term $\kappa h \mathrm{e}^{-\kappa h}$ describes the near-field screening effect of the EDL. As humidity or temperature increases, trace amounts of water and thermal activation significantly enhance the dissociation of AOT [20], thereby increasing the effective ion concentration and $\sigma_{\rm m}$. This reduces the Debye length $\lambda_{\rm D}$, strengthens screening, and causes the dipolar interaction to gradually decay to zero at high $\sigma_{\rm m}$.

2. Rotation-Induced Hydrodynamic Forces $\boldsymbol{F}_{\rm HI}$
   Rotating Quincke rollers also drive the surrounding fluid and interact with each other via long-range HIs [Fig. 4(b)]. For a sphere rotating at $\boldsymbol{\omega}$ in infinite space filled with viscous fluid, the induced flow field at position $\boldsymbol{r}$ can be described as [41]

$$\boldsymbol{u}(\boldsymbol{r}) = \frac{a^3}{r^3}\boldsymbol{\omega}\times\boldsymbol{r}. \tag{5}$$

   Equation (5) suggests that $F_{\rm HI}$ scales with the rollers' angular velocity ω. Because we have experimentally observed that v first increases slightly and then decreases rapidly as T and RH increase and therefore as $\sigma_{\rm m}$ increases [Figs. S4(b) and S4(d) in the SM], and v is approximately equal to ωr without slip (see SM, Movie 2), we conclude that $F_{\rm HI}$ decreases upon increasing T and/or RH.

3. Electrohydrodynamic Forces $\boldsymbol{F}_{\rm EHD}$
   In addition to the flow generated by rotation, Quincke rollers also produce EHD flows [Fig. 4(c)]. EHD flows comprise two main contributions. The first is an electro-osmotic (EO) flow [36] along the solid–liquid interface, originating from ion motion inside the EDL under a tangential electric field. The characteristic slip velocity, $\boldsymbol{u}_{\rm EO}$, of a roller with zeta potential ζ can be estimated by the Henry equation

$$\boldsymbol{u}_{\rm EO} = \frac{2\varepsilon_{\rm m}\xi\boldsymbol{E}_{\rm t}}{3\mu_{\rm m}}f(\kappa a), \tag{6}$$

   where $\boldsymbol{E}_{\rm t}$ is the tangential electric field, and $f(\kappa a)$ is Henry function (see Eq. S18 of the SM).
   The second component of the EHD flow is a bulk flow, $\boldsymbol{u}_{\rm SC}$, caused by the migration of space charges of density $\rho_{\rm e}$ in the medium under the external electric field $\boldsymbol{E}$ [37]. The Stokes equation with the electrical body force $\rho_{\rm e}\boldsymbol{E}$ is [38]

$$\mu_{\rm m}\nabla^2\boldsymbol{u}_{\rm SC} - \nabla p + \rho_{\rm e}\boldsymbol{E} = 0, \tag{7}$$

   where p is the fluid pressure. As $\sigma_{\rm m}$ increases, $\rho_{\rm e}$ around the rollers will increase, which increases $\boldsymbol{u}_{\rm SC}$.

These three forces mentioned above were numerically solved using finite-element simulations in COMSOL Multiphysics [Figs. 5(a)–5(c)], and the total interaction force, $F_{\rm total}$, was obtained between a pair of rollers [Fig. 5(d)]. The detailed simulation method is described in Sect. S2.4 of the SM, while the parameters used in the model were chosen to match the experimental system as closely as possible (see the following Discussion section and Sect. S4 of the SM).

The results in Figs. 5(a)–5(c) show qualitatively different dependencies of the three interactions on $\sigma_{\rm m}$. The net calculated $F_{\rm dip}$ is repulsive across the entire calculated range of $\sigma_{\rm m}$ [Fig. 5(a)]. However, $F_{\rm dip}$ becomes anisotropic for $\sigma_{\rm m} > 20\ \mathrm{nS\cdot m^{-1}}$: $F_{\rm dip}$ is stronger for two rollers aligned perpendicular to their velocity $\boldsymbol{v}$ (i.e., "side-by-side") than for two rollers aligned parallel to $\boldsymbol{v}$ (i.e., "head-to-tail"). As $\sigma_{\rm m}$ increases further, $F_{\rm dip}$ in both cases decreases rapidly because of stronger EDL screening, as suggested by Eqs. (3) and (4). On the other hand, $F_{\rm EHD}$ is attractive across the entire calculated range of $\sigma_{\rm m}$ [Fig. 5(b)], and its magnitude increases with increasing $\sigma_{\rm m}$. In contrast, $F_{\rm HI}$ is weakly repulsive for two rollers arranged "head-to-tail" and practically zero for two rollers arranged "side-by-side" [Fig. 5(c)].

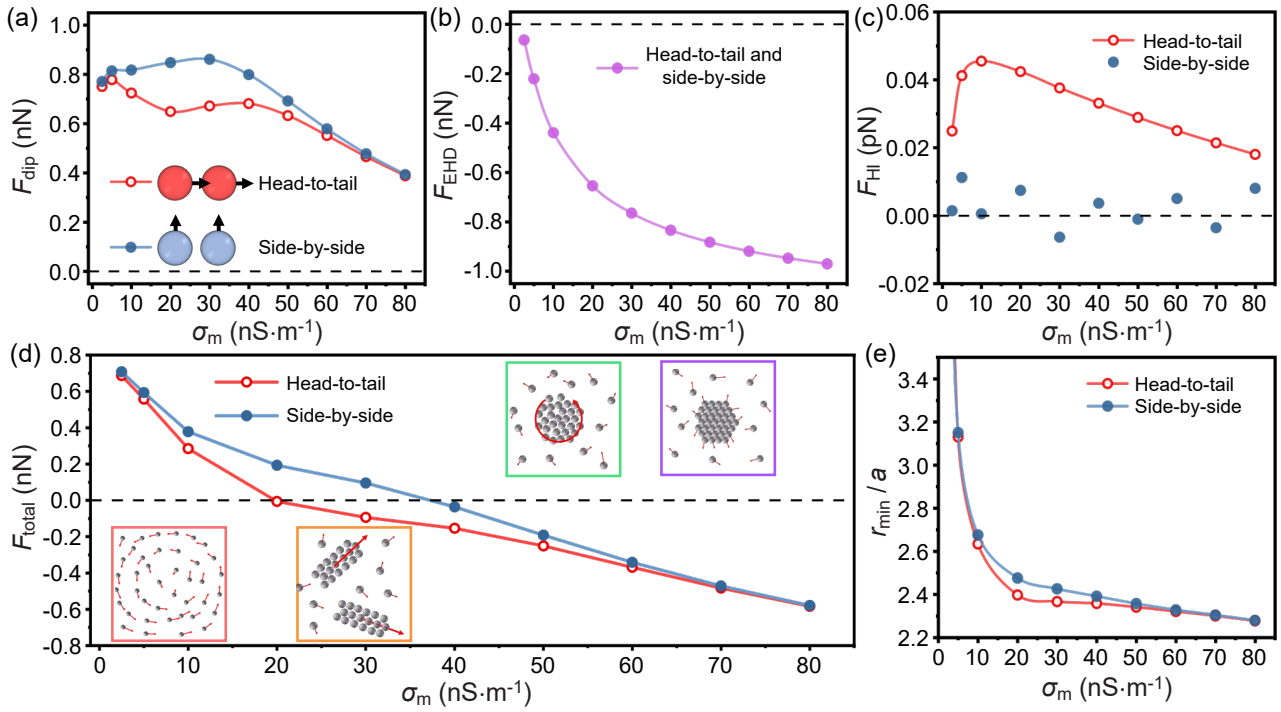

Fig. 5. Calculated pairwise interaction forces between two Quincke rollers: (a) electrical dipolar forces, F_{dip}; (b) hydrodynamic forces from the EHD flows, F_{EHD}; (c) hydrodynamic forces from the rotation of rollers, F_{HI}; and (d) the combined forces, F_{total}, versus σ_m between a pair of rollers aligned parallel to $\boldsymbol{v}$ ("head-to-tail", red open circles) or perpendicular to $\boldsymbol{v}$ ("side-by-side", blue filled circles). The data in (b) are indistinguishable for either alignment. Insets in (d) illustrate the four states of collective behavior observed at different σ_m. (e) Calculated locations of the interaction potential energy minima (r_{min}) between two Quincke rollers. See Fig. S3 of the SM for the full interaction potential energy data. The data points are connected by modified Bézier curves, except for the "side-by-side" configuration in (c).

However, since F_{HI} is around four orders of magnitude smaller than F_{EHD} (0.01–0.05 pN vs. 0.1–1 nN), the latter dominates the flow-induced interactions between Quincke rollers in the calculated range of σ_m. Note that although the rotating flow from one roller does not significantly attract or repel the other rollers, as Fig. 5(c) suggests, it provides the velocity alignment critical for the formation of Quincke roller flocks observed in the vortex, polar cluster, and rotating cluster state [5,15,31,42].

Figure 5(d) shows the overall interaction forces, F_{total}, between two rollers aligned "head-to-tail" or "side-by-side", and provides a qualitative understanding of how humidity and temperature mediate the collective behavior of Quincke rollers. To elaborate, at low RH or low T, where σ_m is low, the system is dominated by repulsive dipolar interactions. Quincke rollers therefore move directionally and repel each other, while hydrodynamic alignment promotes the formation of a large flock. Since the rollers are confined in an oil droplet of finite size, one or multiple vortices form. When σ_m increases above approximately 18 nS·m^{-1} (corresponding to RH ~38% or T ~32 ℃), the interaction becomes increasingly anisotropic: attraction first appears along the rolling direction, while repulsion remains in the transverse direction. As a result, the clusters elongate along the rolling direction, corresponding to the polar cluster state. When σ_m further exceeds about 37 nS·m^{-1} (corresponding to RH ~51% or T ~ 54 ℃), the dipolar repulsion becomes much weaker, and the EHD attraction starts to dominate. Rollers therefore attract isotropically and form compact clusters. These clusters rotate because of a nonreciprocal coupling between their polar alignment and their hexagonal structural order [43,44]. As σ_m continues to increase, the attraction between rollers becomes even stronger, suppressing the motion of rollers inside the crystal and eventually leading to the formation of the active crystal state.

Integrating the interaction forces over distance yields effective interaction potentials (Fig. S3 of the SM), showing that the position of the potential minimum, r_{min}, shifts to shorter particle separations as σ_m increases [Fig. 5(e)]. In addition, at intermediate conductivities (~20–50 nS·m^{-1}), r_{min} is smaller along the rolling direction than in the transverse direction, consistent with the anisotropic structure of polar clusters.

Discussion

Determination of Key Parameters for Calculating Pair Interaction Forces

One of the main contributions of this work is that all interaction forces are calculated explicitly, with each parameter assigned a clear physical meaning and an experimentally relevant value. Among the parameters that play important roles in the pair-interaction calculations, the rollers' angular speed ω, the electric double-layer thickness λ_D, particle zeta potential ζ, and medium electrical permittivity ε_m cannot be determined from existing theory. Instead, they were either obtained experimentally or inferred using minimal assumptions as detailed below.

First, the angular velocity ω not only determines the magnitude of $\boldsymbol{u}_{HI}$ through Eq. (5), but also affects the complex permittivity ε^*, and therefore the Clausius-Mossotti factor K, the effective dipole moment $\boldsymbol{p}_{eff}$, and its tilt angle α (Eqs. S3–S7 of the SM). As a result, ω is a key input parameter in the calculation of F_{dip} at varying σ_m. We have therefore fitted ω against σ_m with an empirical equation (Eq. S14 of the SM).

Second, weak dissociation of AOT in the nonpolar solvent hexadecane produces an EDL around the particle surface. Estimating λ_D requires the effective ion concentration in the medium, which is difficult to measure directly. At an AOT concentration of 0.15 M, AOT is known to form univalent charged reverse micelles [45]. We estimated the ion concentration from the measured conductivity and the electrophoretic mobility of the micelles [45–47] following Eqs. S14 and S15 of the SM. The calculated Debye length, λ_D, is about 0.85 μm for σ_m = 10 nS·m^{-1} (see Sect. S4.2 of the SM).

Third, the roller's zeta potential ζ is important for EDL structure

and for calculating the magnitude of $\boldsymbol{u}_{EO}$ via Eq. (6). The value of ζ was obtained from electrophoresis measurements rather than the dynamic light scattering (DLS) method typically used for microspheres, because DLS was not suitable for a liquid of low σ, such as hexadecane [48]. Specifically, a direct-current electric field was first applied to a particle suspension in AOT-hexadecane sandwiched between two indium tin oxide electrodes to drive the particles toward the high-potential electrode surface. The field direction was then reversed, causing the particles to detach from the electrode and migrate electrophoretically toward the opposite side (see SM, Movie 3). By measuring the electrophoretic velocity in Eq. (6), the particle zeta potential was determined to be −10.4 mV (see Sect. S4.3 of the SM).

Fourth, ε_m of the Quincke roller suspension is often simply assumed to be around $2\varepsilon_0$ [7,15]. However, this value corresponds to pure hexadecane. Instead, ε_m of 0.15 M AOT-hexadecane was experimentally determined to be around $7\varepsilon_0$, and this value is larger than $2\varepsilon_0$ because AOT is a polar molecule and increases the permittivity of hexadecane. ε_m further increases by 9.6% and 14.2% as T and RH rise, respectively. In the simulations, we therefore use $\varepsilon_m = 7.18\varepsilon_0$, obtained by averaging the values of ε_m at different RH from Fig. 3(a).

Overall, we avoid introducing unnecessary assumptions and rely as much as possible on experimentally measured quantities and values reported in the previous literature. Although some uncertainty remains, such as the detailed structure of the EDL and the neglect of the tilt of dipole in the EHD calculations, these factors mainly affect the magnitude of the interactions rather than the qualitative collective behaviors.

Other Parameters Affected by Temperature and Humidity

Our calculations above have focused exclusively on the change in the medium's electrical properties induced by humidity and temperature. However, temperature changes could also affect other physical quantities besides σ_m and ε_m, such as the medium viscosity μ_m and the EDL thickness λ_D. We have experimentally determined a decrease in μ_m from 3.2 mPa·s to 2.3 mPa·s by increasing T from 20 ℃ to 60 ℃ (Fig. S5 of the SM), a much smaller relative change than that in σ_m. On the other hand, at fixed effective ion concentration, an increase in T from 20 ℃ to 60 ℃ would, in theory, increase λ_D by 6.6% following $\lambda_D \propto (k_B T)^{1/2}$, and further decrease the screening factor $\kappa h e^{-\kappa h}$ by 11.8%. This change in $\kappa h e^{-\kappa h}$ and thus in the magnitude of F_{dip} causes the F_{total} of two rollers to become negative at around $\sigma_m = 33$ nS·m^{-1} instead of 37 nS·m^{-1} for the "side-by-side" arrangement. However, this effect only introduces a small quantitative shift and does not change the overall evolution of the collective behavior.

Conclusion

In summary, we have demonstrated that environmental temperature and humidity can regulate the collective behavior of Quincke rollers. As the RH increases from 5% to 65%, the electrical conductivity of the medium σ_m increases significantly, from about 2.7 nS·m^{-1} to about 79.6 nS·m^{-1}, or from 4.7 nS·m^{-1} to 46.8 nS·m^{-1} as the temperature rises from 20 ℃ to 60 ℃. Quantitative modeling reveals that, at low σ_m, the pairwise interaction is dominated by electrical dipolar repulsion, so that rollers form large vortices of separated rollers aligned by directional flows. As σ_m increases, dipolar repulsion decreases while EHD flows increasingly cause rollers to attract. The attraction is anisotropic at an intermediate σ_m, stronger along the rolling direction than in the transverse direction, leading to polar clusters. The attraction becomes isotropic when σ_m is further increased, leading to rotating clusters and, ultimately, active crystals at even higher σ_m. A population of Quincke rollers therefore successively transitions from vortices to polar clusters to rotating clusters and, finally, to active crystals as temperature or humidity increases.

Moreover, these findings explain the empirical, puzzling observation that Quincke rollers preferentially form vortices under winter-like low-temperature and low-humidity conditions, but tend to form clusters under summer-like high-temperature and high-humidity conditions. This work further establishes ambient conditions as a simple and effective handle to tune the collective behaviors of Quincke rollers. Furthermore, we have developed a quantitative framework, with experimentally determined parameters, to compute the dipolar, HI, and EHD interactions of two Quincke rollers, enabling predictive description of their collective-state evolution. These results provide a general route for controlled manipulation of Quincke roller systems and offer broader implications for soft and active matter.

Acknowledgements

This work was supported by the National Natural Science Foundation of China (Grant Nos. T2322006 and 12674257 for W.W., Z.Q., J.G., J.L., and G.W., Grant Nos. 12574223 and 12347102 for B.Z. and H.L.), the China Manned Space Engineering Program (Project No. KJZ-YY-NLT0502 for W.W., Z.Q., J.G., J.L., and G.W.), and the Shenzhen Science and Technology Program (Grant No. RCYX20210609103122038).

References

[1] Needleman D and Dogic Z 2017 *Nat. Rev. Mater.* **2** 17048
[2] Baulin V A, Giacometti A, Fedosov D A, Ebbens S, Varela-Rosales N R, Feliu N, Chowdhury M, Hu M, Füchslin R, Dijkstra M, Mussel M, Van Roij R, Xie D, Tzanov V, Zu M, Hidalgo-Caballero S, Yuan Y, Cocconi L, Ghim C M, Cottin-Bizonne C, Miguel M C, Esplandiu M J, Simmchen J, Parak W J, Werner M, Gompper G, and Hanczyc M M 2025 *Soft Matter* **21** 4129
[3] Marchetti M C, Joanny J F, Ramaswamy S, Liverpool T B, Prost J, Rao M, and Simha R A 2013 *Rev. Mod. Phys.* **85** 1143
[4] Zhang H P, Be'er A, Florin E L, and Swinney H L 2010 *Proc. Natl. Acad. Sci. USA* **107** 13626
[5] Zheng J, Chen J, Jin Y, Wen Y, Mu Y, Wu C, Wang Y, Tong P, Li Z, Hou X, and Tang J 2023 *Nature* **617** 499
[6] Yan J, Han M, Zhang J, Xu C, Luijten E, and Granick S 2016 *Nat. Mater.* **15** 1095
[7] Pradillo G E, Karani H, and Vlahovska P M 2019 *Soft Matter* **15** 6564
[8] Morin A, Desreumaux N, Caussin J B, and Bartolo D 2016 *Nat. Phys.* **13** 63
[9] Zhang B, Yuan H, Sokolov A, De La Cruz M O, and Snezhko A 2021 *Nat. Phys.* **18** 154
[10] Liu Z T, Shi Y, Zhao Y, Chaté H, Shi X Q, and Zhang T H 2021 *Proc. Natl. Acad. Sci. USA* **118** e2104724118
[11] Jones T B 1984 *IEEE Trans. Ind. Appl.* **IA-20** 845
[12] Zhang B, Glatz A, Aranson I S, and Snezhko A 2023 *Nat. Commun.* **14** 7050
[13] Bricard A, Caussin J B, Desreumaux N, Dauchot O, and Bartolo D 2013 *Nature* **503** 95
[14] Zhang B, Hilton B, Short C, Souslov A, and Snezhko A 2020 *Phys. Rev. Res.* **2** 043225
[15] Bricard A, Caussin J B, Das D, Savoie C, Chikkadi V, Shitara K, Chepizhko O, Peruani F, Saintillan D, and Bartolo D 2015 *Nat. Commun.* **6** 7470
[16] Karani H, Pradillo G E, and Vlahovska P M 2019 *Phys. Rev. Lett.* **123** 208002
[17] Zhang B, Snezhko A, and Sokolov A 2022 *Phys. Rev. Lett.* **128** 018004
[18] Imamura S, Sawaki K, Molina J J, Turner M S, and Yamamoto R 2023 *Adv. Theory Simul.* **6** 2200683
[19] Mauleon-Amieva A, Mosayebi M, Hallett J E, Turci F, Liverpool T B, Van Duijneveldt J S, and Royall C P 2020 *Phys. Rev. E* **102** 032609
[20] Haandrikman G, Daane G J R, Kerkhof F J M, Van Os N M, and Rupert L A M 2002 *J. Phys. Chem.* **96** 9061
[21] López Llobet L 2020 *The Important Role of Electrohydrodynamics in a System of Quincke Rollers* [D] (Bachelor's thesis, Universitat de Barcelona)
[22] Zhang B and Snezhko A 2022 *Phys. Rev. Lett.* **128** 218002
[23] Zhang Z, Yuan H, Dou Y, De La Cruz M O, and Bishop K J M 2021 *Phys. Rev. Lett.* **126** 258001

[24] Leyva S G, Zhang Z, Olvera De La Cruz M, and Bishop K J M 2026 *Nat. Commun.* **17** 1841
[25] Zhang Z, Yuan H, Dou Y, De La Cruz M O, and Bishop K J M 2021 *Phys. Rev. Lett.* **126** 258001
[26] Basu H S, Jena S K, and Kondaraju S 2024 *Phys. Fluids* **36** 102125
[27] Sasikala T S and Sebastian M T 2015 *J. Electron. Mater.* **45** 729
[28] Liu D, Ma J, Cheng H, and Zhao Z 1998 *Colloids Surf. A: Physicochem. Eng. Asp.* **135** 157
[29] Mehta S K and Sharma S 2006 *J. Colloid Interface Sci.* **296** 690
[30] Eicke H F, Borkovec M, and Das-Gupta B 2002 *J. Phys. Chem.* **93** 314
[31] Lu S Q, Zhang B Y, Zhang Z C, Shi Y, and Zhang T H 2018 *Soft Matter* **14** 5092
[32] Dolinsky Y and Elperin T 2012 *Phys. Rev. E* **85** 026608
[33] Wang Z, Miksis M J, and Vlahovska P M 2023 *Soft Matter* **19** 7663
[34] Du H, Zhou X, Ni Q, Chen K, Tian W, and Zhang T 2025 *Acta Phys. Sin.* **74** 116401
[35] Yeh S R, Seul M, and Shraiman B I 1997 *Nature* **386** 57
[36] Swan J W and Furst E M 2012 *J. Colloid Interface Sci.* **388** 92
[37] Vasilkov S A, Chirkov V A, and Stishkov Y K 2017 *Phys. Fluids* **29** 063601
[38] Zhakin A I 2012 *Phys.-Usp.* **55** 465
[39] Xie Z, Dong Q, Wang Z, Zhao X, and Hu G 2024 *Phys. Fluids* **36** 127146
[40] Sainis S K, Merrill J W, and Dufresne E R 2008 *Langmuir* **24** 13334
[41] Box F, Thompson A B, and Mullin T 2015 *Exp. Fluids* **56** 209
[42] Das D and Saintillan D 2023 *Soft Matter* **19** 6825
[43] Kole S J, Chao X, Mauleon-Amieva A, Hanai R, Royall C P, and Liverpool T B 2025 arXiv:2501.15996 [cond-mat.soft]
[44] Mauleon-Amieva A, Liverpool T B, Williams I, Souslov A, and Royall C P 2025 *Soft Matter* **21** 7155
[45] Hsu M F, Dufresne E R, and Weitz D A 2005 *Langmuir* **21** 4881
[46] Shaparenko N O, Kompan'kov N B, Demidova M G, and Bulavchenko A I 2020 *Electrophoresis* **41** 1592
[47] Morrison I D 1993 *Colloids Surf. A: Physicochem. Eng. Asp.* **71** 1
[48] Patel M N, Smith P G, Kim J, Milner T E, and Johnston K P 2010 *J. Colloid Interface Sci.* **345** 194